# Role of Surface/Interfacial Cu(2+) Sites in the Photocatalytic Activity of Coupled CuO-TiO(2) Nanocomposites

**ARTICLE** *in* THE JOURNAL OF PHYSICAL CHEMISTRY C · DECEMBER 2008

Impact Factor: 4.77 · DOI: 10.1021/jp8068392

# Role of Surface/Interfacial $Cu^{2+}$ Sites in the Photocatalytic Activity of Coupled $CuO-TiO_2$ Nanocomposites

**Gonghu Li,[†,§] Nada M. Dimitrijevic,[‡] Le Chen,[†] Tijana Rajh,[‡] and Kimberly A. Gray*[,†]**

*Institute for Catalysis in Energy Processes, Department of Civil and Environmental Engineering, Northwestern University, Evanston, Illinois 60208, and Chemical Sciences and Engineering Division, Center for Nanoscale Materials, Argonne National Laboratory, Argonne, Illinois 60439*

*Received: July 31, 2008; Revised Manuscript Received: September 19, 2008*

Coupled $CuO-TiO_2$ nanocomposite photocatalysts were prepared by a deposition precipitation method and were characterized with a variety of techniques. Electron paramagnetic resonance (EPR) spectroscopy was employed to study the local structures of surface/interfacial $Cu^{2+}$ sites using $Cu^{2+}$ as a sensitive paramagnetic probe. The addition of bulk CuO to $TiO_2$ led to decreased photocatalytic efficiency in the degradation of methylene blue. However, doping with a very small amount of CuO (0.1 wt % copper loading) significantly enhanced the photocatalytic activity of $TiO_2$. EPR study of the $TiO_2$ surface revealed the presence of both highly dispersed CuO clusters and substitutional $Cu^{2+}$ sites (Ti−O−Cu linkages) at 0.1 wt % copper loading. The data suggest that the Ti−O−Cu linkages contributed to the improved photooxidative activity of the 0.1% $CuO-TiO_2$ nanocomposite. In contrast, at higher loadings the bulk form of CuO created charge recombination centers lowering the photoactivity of the composites.

## 1. Introduction

The photoactivation of wide-band semiconductors has been and continues to be extensively investigated due to their many applications including environmental photocatalysis and solar energy conversion.[1−5] Titania-based nanocomposites exhibit enhanced photocatalytic properties that arise, in part, from the interaction between different crystallites and/or electronic coupling between $TiO_2$ and the other phase.[6,7] For example, noble metals such as Pt deposited on $TiO_2$ surface can act as the sink for photoexcited electrons, hindering the recombination of charge carriers (electrons and holes).[8] Interparticle transfer of charge carriers contributes to the enhanced photocatalytic efficiency of coupled semiconductors when the energies of valence and conduction bands are properly matched.[9,10]

In addition to the energetic consideration, the attachment (interfacial morphology) between phases represents another essential factor influencing the photocatalytic activities of $TiO_2$-based nanocomposites.[6] In general, certain interfacial morphologies and crystal faces are required for considerable synergistic effects to occur between two components.[11] For instance, Gray and co-workers demonstrated that the existence of a particular nanostructured morphology of interwoven rutile and anatase crystallites promotes spatial charge separation and accounts for the improved photocatalytic activity of mixed-phase $TiO_2$ materials such as Degussa P25.[12−14] In this study, we explore the role of surface/interfacial $Cu^{2+}$ sites in the photocatalytic activity of coupled $CuO-TiO_2$ nanocomposites. Since the band edges of $TiO_2$ bracket those of CuO (Figure 1, inset), photoexcited charge carriers in $TiO_2$ may transfer to and ultimately recombine in CuO. In the absence of sacrificial agents as electron or hole scavengers, the addition of bulk CuO to $TiO_2$ would lead to decreased photocatalytic efficiency. This was observed in the photocatalytic degradation of methylene blue (MB) under UV irradiation (Figure 1). However, we discovered that doping $TiO_2$ with a very small amount of CuO (0.1 wt % copper loading) significantly increased the photocatalytic efficiency of $TiO_2$.

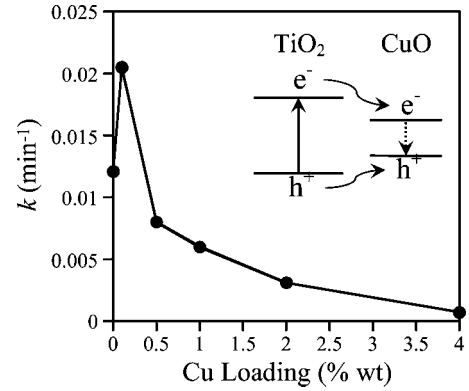


**Figure 1.** First-order rate constants ($k$ in $min^{-1}$) as measured by methylene blue degradation under UV irradiation. Synthesized $CuO-TiO_2$ nanocomposites with different copper loadings were used as the photocatalysts. Inset: a schematic diagram showing the photoinduced charge separation ($e^-$ in conduction band and $h^+$ in valence band) in $TiO_2$, charge transfer from $TiO_2$ to CuO and subsequent charge recombination in CuO (dotted arrow). The difference between the conduction band edges of $TiO_2$ and CuO is estimated to be 0.75 eV.[15]

There usually exist optimal loadings for coupled semiconductors as photocatalysts. For example, Slamet and co-workers studied the photocatalytic reduction of $CO_2$ on $CuO-TiO_2$ nanocomposites; a composite photocatalyst with 3 wt % copper demonstrated the highest activity for methanol production by $CO_2$ reduction.[16] A "shading effect", in which colored CuO absorbs light and reduces the photoexciting capacity of $TiO_2$, was invoked to explain the detrimental effect of Cu doping

* To whom correspondence should be addressed. Phone: (+1) 847 4674252. Fax: (+1) 847 4914011. E-mail: k-gray@northwestern.edu.
† Northwestern University.
‡ Argonne National Laboratory.
§ Current address: Department of Chemistry, Yale University, New Haven, CT 06520.

10.1021/jp8068392 CCC: $40.75 
Published on Web 11/08/2008

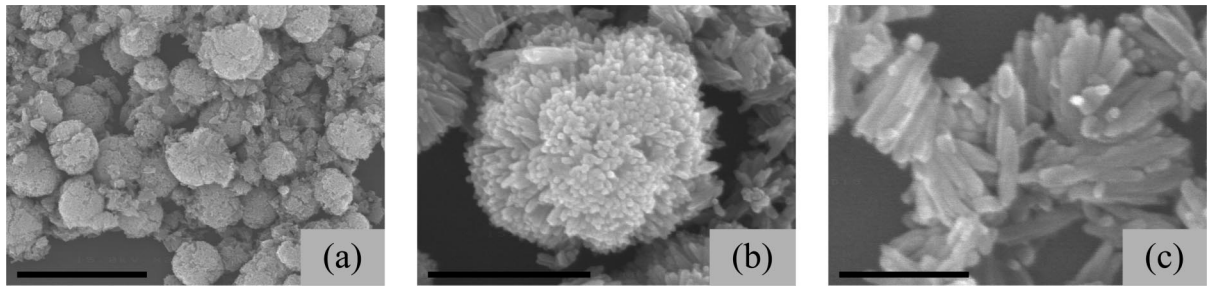


**Figure 2.** Electron micrographs of 4% $CuO-TiO_2$ at different magnification. Scale bars are (a) 2 $\mu$m, (b) 500 nm, and (c) 200 nm.

beyond the optimum.[16] Tseng and co-workers demonstrated that 2 wt % was the optimal loading for copper-doped $TiO_2$ photocatalysts.[17,18] Since electron paramagnetic resonance (EPR) spectroscopy is a highly sensitive tool for studying paramagnetic transition metal ions,[19] in this study we investigate the local structures of surface/interfacial $Cu^{2+}$ sites using EPR and explain the enhancement in the photocatalytic properties of the 0.1% $CuO-TiO_2$ nanocomposite. This study also represents an example of our recent attempts to screen $TiO_2$-based nanocomposites which have optimized interfacial morphologies and potential energy applications.

## 2. Experimental Methods

**Materials Synthesis.** Rutile $TiO_2$ nanocrystals were synthesized via a low-temperature hydrothermal method.[20] Prior to the hydrothermal process, 10 mL of titanium (IV) chloride ($TiCl_4$, Sigma-Aldrich, 99.9%) were hydrolyzed in 100 mL of Milli-Q water, forming a clear solution after stirring at room temperature for 90 min. The clear solution was then transferred to a 250 mL flask and was refluxed at 373 K for 22 h. The obtained $TiO_2$ nanocrystals were washed with water and mixed with a specific amount of $Cu(NH_3)_4^{2+}$ ions prepared from cupric sulfate ($CuSO_4 \cdot 5H_2O$, Mallinckrodt Chemicals, 98%) and ammonium hydroxide ($NH_4OH$, Fisher Scientific). The mixture was stirred at 293 K for 30 min prior to the addition of a solution of 2% hydrogen peroxide ($H_2O_2$, Mallinckrodt Chemicals). The resulting suspension was further stirred for 30 min, leading to the deposition of Cu(0) on $TiO_2$ nanocrystals according to the following reaction.[21]

$$Cu(NH_3)_4^{2+} + H_2O_2 + 2OH^- \rightarrow Cu + O_2 + 4NH_3 + 2H_2O \quad (1)$$

The synthesized $TiO_2$ nanocrystals were separated from the suspension by centrifugation, washed with water, and dried at 353 K. Cu(0) deposited on $TiO_2$ was further oxidized to Cu(II) by sintering at 773 K in air for 4 h (ramp rate 5 K/min). The synthesized nanocomposites are denoted as $x$% $CuO-TiO_2$ where $x$ stands for the weight fraction of copper on $TiO_2$. The loading of copper (0.1, 0.5, 1, 2, and 4 wt %) was controlled by the amount of $Cu(NH_3)_4^{2+}$ ions used during the synthesis process. Following the same procedure, a pure $TiO_2$ sample (Rutile $TiO_2$) was also prepared without the use of cupric sulfate.

**Materials Characterization.** The BET surface areas of synthesized materials were measured with an Autosorb 1-MP from Quantachrom Instruments. The X-ray diffraction (XRD) patterns of powder samples were recorded on a Rigaku XDS 2000 diffractometer using nickel-filtered Cu K$\alpha$ radiation ($\lambda$ = 1.5418 Å) over the range of $20° < 2\theta < 60°$. A Hitachi S-4500 SEM equipped with a cold field emission electron gun was used to examine the synthesized nanocomposites. The optical spectra of the nanocomposites were recorded with a diffuse reflectance attachment on a Cary 1E UV−visible spectrophotometer. The chemical states of Ti and Cu were examined using an X-ray photoelectron spectrometer on an Omicron ESCA Probe. EPR spectra were collected on a Bruker Elexys E580 spectrometer equipped with a helium cryostat. In EPR studies, samples dispersed in Milli-Q water were purged with argon, cooled to 4.5 K, and illuminated within the cavity at that temperature while spectra were acquired. A 300 W xenon lamp (ILC Inc.) was used as the light source for EPR studies. For visible light experiments, the lamp was filtered by a Schott 400 nm long-pass filter. The $g$ tensor values were calibrated for homogeneity and accuracy by comparing to a coal standard ($g = 2.00285 \pm 0.00005$).

**Photocatalytic Testing.** The photodegradation of methylene blue (MB) was carried out in a batch reactor, in which 30 mg of photocatalyst were mixed with a 100 mL solution of 5 mg/L MB (Merck, USP). The slurry was stirred in the dark for 10 min and then subject to UV irradiation provided by a 100 W mercury spot lamp (UVP Inc.), which has a strong emission peak at 366 nm. The photon flux at the solution surface was measured to be 150 $\mu M/m^2 \cdot s$. For visible light experiments, the slurry was covered with a long-pass filter (Edmund Industrial Optics, Absorbance is 0.96 at 398 nm); an ordinary incandescent lamp was used as the visible light source, providing irradiance with an intensity of 75 W $m^2$ and a peak wavelength around 520 nm.[22] Every 5 min the reaction solution was sampled and separated from the photocatalyst using a GHP Acrodisc 13 mm syringe filter (Pall). The absorbance of MB at 660 nm was monitored using a Hitachi U-2000 UV−visible spectrophotometer. According to Beer's law, the concentration of MB is proportional to its absorbance at 660 nm. First-order rate constants ($k$) were obtained by fitting the data obtained in MB degradation to the following equation,

$$\ln(C_t/C_0) = -kt \quad (2)$$

where $C_0$ and $C_t$ represent the concentrations of MB in the beginning of photodegradation and at reaction time $t$, respectively.

## 3. Results and Discussion

**Characterization of $CuO-TiO_2$ Nanocomposites.** During the hydrolysis of $TiCl_4$ as the titanium precursor, a large amount of hydrochloric acid was generated in the solution. Subsequent hydrothermal synthesis under the acidic condition resulted in the formation of pure-phase rutile nanocrystals, as determined by XRD.[20] In this study, the synthesis of rutile nanocrystals did not involve the use of any organic solvent. The deposition of copper did not affect the primary morphology or aggregation state of synthesized $TiO_2$ nanocrystals to any appreciable extent, nor did the crystal phase of $TiO_2$ nanocrystals change with loading copper by the deposition precipitation method. Figure 2 shows the typical SEM images of 4% $CuO-TiO_2$. Upon

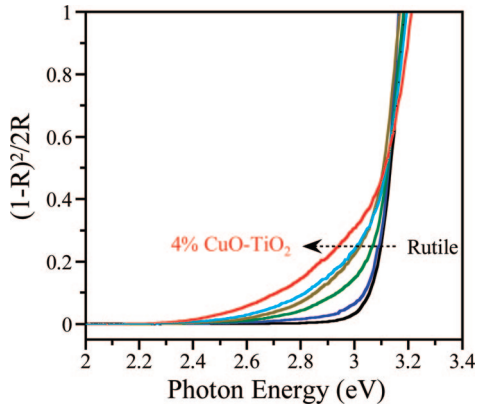


**Figure 3.** Optical spectra of CuO−$TiO_2$ nanocomposites with different copper loadings (from right to left: Rutile, 0.1%, 0.5%, 1%, 2%, and 4% CuO−$TiO_2$, respectively). The *y* axis is expressed in Kubelka−Munk unit (*R*, reflectance).

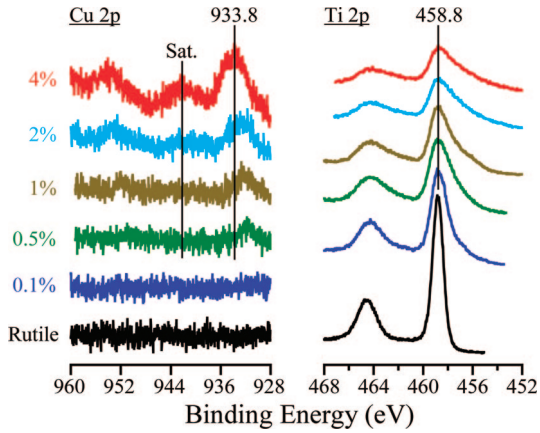


**Figure 4.** Cu 2p and Ti 2p XPS spectra of CuO−$TiO_2$ nanocomposites with different copper loadings (Sat., shakeup satellite peak).

drying at 353 K and sintering at 773 K, most of the rutile nanocrystals formed spherical, micron-sized aggregates. These aggregates are composed of mostly rodlike, individual rutile nanocrystals.

Doping with CuO increased the surface areas of synthesized $TiO_2$ nanoparticles. The specific surface areas were 22.6, 23.7, 25.9, and 33.8 $m^2/g$ for 0% (pure $TiO_2$), 0.1%, 0.5%, and 4% CuO−$TiO_2$, respectively. However, the formation of CuO could not be detected, even at the highest copper loading (4 wt %), with XRD or SEM. Rather, the existence and identity of copper species in the synthesized nanocomposites was investigated with more sensitive techniques, including UV−visible, XPS, and EPR spectroscopies. Doping with transition metal ions usually extends the optical absorptions of $TiO_2$ materials into the visible light region.[23] Figure 3 shows the optical spectra of synthesized $TiO_2$ nanocomposites. It can be inferred from the spectra that the Rutile $TiO_2$ has a bandgap ($E_{bg}$) around 3.1 eV. The copper-loaded $TiO_2$ nanocomposites have photoresponses between 2.2 and 3.1 eV, which grows as the copper loading increases from 0.1 to 4 wt %. The optical spectra shown in Figure 3 indicate the existence of CuO ($E_{bg}$ = 1.7 eV) or $Cu_2O$ ($E_{bg}$ = 2.2 eV) in the synthesized nanocomposites.[15]

**XPS of CuO−$TiO_2$ Nanocomposites.** XPS was utilized to analyze the chemical states of Cu and Ti in the synthesized nanocomposites. The core level XPS peaks of Cu 2p and Ti 2p are shown in Figure 4. The Cu $2p_{3/2}$ transition with a binding energy around 933.8 eV is seen for the nanocomposites with copper loadings greater than 0.5% (Figure 4). This and the shakeup satellite peak around 942.3 eV clearly indicate the existence of fully oxidized CuO.[24−27]

The peak intensity of the Cu $2p_{3/2}$ transition becomes greater as the copper loading increases from 0.5 to 4 wt % (Figure 4). This is consistent with the presence of copper species that accounts for the significant photoresponse of CuO−$TiO_2$ nanocomposites below 3.1 eV (Figure 3). It should be noted that this Cu $2p_{3/2}$ transition shifts to lower binding energies as the copper loading decreases. This indicates that the $Cu^{2+}$ ions exist in a more dispersed state at lower copper loadings since highly dispersed $Cu^{2+}$ species have lower binding energies than bulk $Cu^{2+}$ in CuO.[26,27]

Although a discernible Cu $2p_{3/2}$ peak is absent from the XPS spectrum of 0.1% CuO−$TiO_2$, the existence of copper species in the nanocomposite can be derived from its Ti 2p XPS spectrum. As shown in Figure 4, the Ti $2p_{3/2}$ transition with a binding energy at 458.8 eV for 0.1% CuO−$TiO_2$ is much broader than that for the Rutile $TiO_2$. The peak broadening, which is due to the existence of multiple Ti species and strong electronic interaction between Cu and Ti in the nanocomposites,[28] is more significant at higher copper loadings. The broad shoulder with binding energies lower than 458.8 eV indicates the existence of Ti in oxidation states lower than 4+.[29−31]

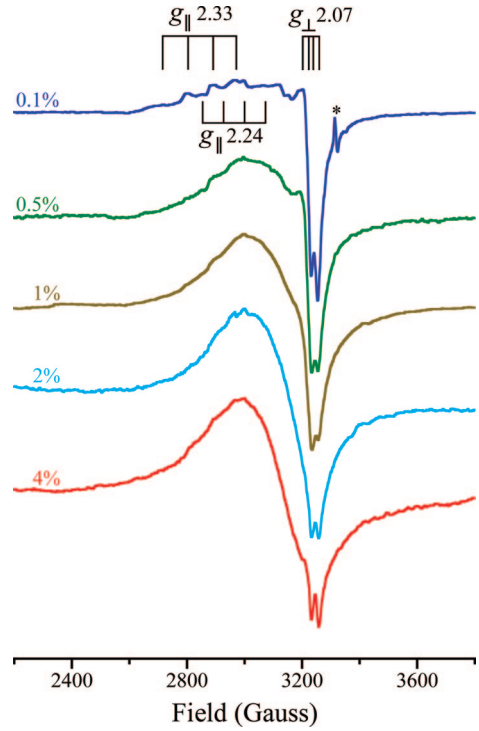


**Figure 5.** Normalized X-band EPR spectra of CuO−$TiO_2$ nanocomposites with different copper loadings. The spectra were recorded in dark at 4.5 K (modulation amplitude 10 G, power 0.003 mW). In the spectrum of 0.1% CuO−$TiO_2$, a sharp resonance ($g$ = 2.005) is denoted with asterisk and is assigned to oxygen vacancies.

**EPR Spectroscopy of CuO−$TiO_2$ Nanocomposites.** The EPR spectra of CuO−$TiO_2$ nanocomposites are presented in Figure 5. In the spectra corresponding to lower concentrations of a CuO (≤0.5%) hyperfine structure due to $I$ = 3/2 of $Cu^{2+}$ ion can be seen. As the CuO concentration increases, the long-range dipolar interactions between $Cu^{2+}$ ions in CuO clusters cause broadening of spectral lines which results in diminished appearance of the anisotropic hyperfine structure.[32−35] From the spectrum of 0.1% CuO−$TiO_2$ it is evident that there are at least two $Cu^{2+}$ species with the values for parallel components of $g_{||}$ = 2.33 and $g_{||}$ = 2.24, both having $A_{||} \approx$ 100 G hyperfine

splitting. The value for the normal component of $g$-tensor is found to be $g_\perp = 2.07$ and cannot be resolved for the two $Cu^{2+}$ ions present in the nanocomposite. In both cases the values of $g_\parallel$ and $g_\perp$ satisfy the relation $g_\parallel > g_\perp > g_e = 2.0023$ ($g_e$ represents the $g$-factor for a free electron) indicating that the $Cu^{2+}$ ions are coordinated by six ligand atoms in an axially distorted octahedron.

The component having resonance parameters $g_\parallel = 2.33$ and $g_\perp = 2.07$ can be assigned to $Cu^{2+}$ ions at substitutional cation sites of $TiO_2$. The $g$ values of this copper species suggest the existence of $Cu^{2+}$ occupying sites vacated by lattice $Ti^{4+}$ ions.[36,37] We propose that due to the thermal treatment at 773 K in our synthesis procedure some of the $Cu^{2+}$ ions replaced surface $Ti^{4+}$ sites. In the matrix of $TiO_2$ network, the substitution of one tetravalent Ti site with one divalent copper ion causes a charge imbalance. For charge compensation to occur, the formation of oxygen defects should accompany this substitution. A sharp resonance signal (denoted with asterisk in Figure 5) with $g = 2.005$ is associated with oxygen vacancies. The same signals due to the formation of oxygen vacancies and/or $O_2^-$ sited on surface oxygen vacancies are observed upon heat treatment of copper complexes in the matrix of silicate glasses or on the surfaces of $SnO_2$.[38,39]

The second component with resonance parameters $g_\parallel = 2.24$ and $g_\perp = 2.07$ corresponds to the $Cu^{2+}$ ions in CuO clusters.[32] As the CuO content rises, the number of isolated clusters and/or the size of CuO clusters increases, resulting in more poorly defined hyperfine resolution. At the same time, the effect of dipolar interaction increases, as well as the ligand field fluctuates, both contributing to the broadening of individual lines.

The illumination of $CuO-TiO_2$ nanocomposites with either visible light only or UV/visible light led to the decrease of $Cu^{2+}$ signal, as observed by EPR for all samples with various copper loadings. Since CuO is a p-type semiconductor (bandgap 1.7 eV),[15] the decrease in intensity for the $Cu^{2+}$ signal upon illumination is due to the trapping of photoexcited electrons in $Cu^{2+}$ sites, forming EPR silent $Cu^+$ sites. It is noteworthy that the synthesized $CuO-TiO_2$ nanocomposites did not demonstrate appreciable photocatalytic activity in MB degradation under visible light irradiation, although photoinitiated charge formation and separation was observed for CuO, a narrow band semiconductor. This indicates that the CuO phase in the synthesized nanocomposites was not photocatalytically active in the degradation of MB.

Furthermore, the conduction band edge for CuO is more positive than that of $TiO_2$ (Figure 1, inset); photoexcited electrons in $TiO_2$ upon UV excitation may transfer to CuO resulting in the reduction of $Cu^{2+}$ to $Cu^+$ and subsequently the decrease of $Cu^{2+}$ EPR resonance signal. After turning off the illumination, the $Cu^{2+}$ EPR signal quickly recovered in dark, indicating fast charge recombination in CuO. However, illumination of the 0.1% $CuO-TiO_2$ nanocomposite results in, at least partial, trapping of electrons in $TiO_2$ lattice, as observed by EPR spectroscopy. Figure 6 presents typical spectra of 0.1% $CuO-TiO_2$. The resonance peak with $g = 1.975$ corresponds to the photogenerated electrons localized at Ti sites in the bulk of a rutile lattice, $(Ti^{3+})_{latt}$.[40,41] The accompanying decrease in a signal with $g = 2.005$ suggests localization of holes at interfacial $TiO_2-CuO$ sites. At higher copper loadings (≥0.5 wt % in this study), no photogenerated electrons were observed at rutile lattice trapping sites. One may explain this by the "shading effect", in which colored CuO absorbs light and reduces the photoexcitation capacity of $TiO_2$.[16] In our opinion, effective electron transfer from the conduction band of $TiO_2$ to

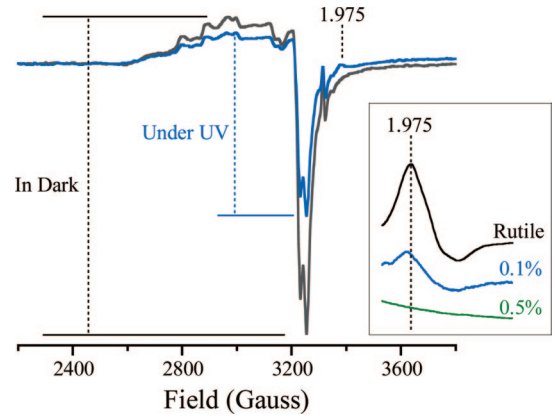


**Figure 6.** EPR spectra of 0.1% $CuO-TiO_2$ acquired in dark (gray line) and under continuous UV/visible light illumination (blue line). Inset: EPR signatures of electron trapping sites ($g = 1.975$) in Rutile $TiO_2$, 0.1% $CuO-TiO_2$, and 0.5% $CuO-TiO_2$. The EPR signatures of electron trapping sites were obtained by subtracting the EPR spectra in dark from the corresponding spectra under continuous UV/visible light illumination.

CuO led to the absence of $Ti^{3+}$ (trapped electrons) in $CuO-TiO_2$ at high CuO loadings. Such interfacial electron transfer is plausible considering the strong electronic interaction between CuO and $TiO_2$ in close proximity, as demonstrated by the XPS results shown in Figure 4. At a very low copper loading (0.1 wt % in this study), the quantity of CuO is insufficient for the complete scavenge of photoexcited electrons in $TiO_2$ to occur. In addition, CuO species exist as highly dispersed clusters in 0.1% $CuO-TiO_2$. Charge transfer kinetics between $TiO_2$ and such highly dispersed CuO clusters may differ significantly from those between $TiO_2$ and bulk CuO nanocrystallites.

**Interfacial Sites in $CuO-TiO_2$ Nanocomposites.** Single-site photocatalytic solids with well-defined, spatially separated active centers have shown great promise for applications including environmental abatement and solar fuel generation.[42] Open-structure solids such as mesoporous silica and zeolites are the most common supports for active photocatalysts. For example, tetrahedrally coordinated Ti sites, which demonstrated excellent photocatalytic activity for NO decomposition and $CO_2$ reduction,[42] were usually prepared in confined environments such as zeolite pores or dispersed onto silica substrates. Interfacial Ti−O−Si linkages have been shown to play an important role in altering the catalytic properties of $TiO_2-SiO_2$ binary oxides.[43−46] In the pioneering work by Frei and co-workers, binuclear metal-to-metal charge transfer moieties such as Ti−O−Cu and Zr−O−Cu were assembled in mesoporous silicate sieve as active sites for solar fuel applications.[47,48] Hashimoto and co-workers assembled Ti−O−Ce bimetallic moieties in mesoporous silica which operated as photocatalysts under visible light illumination.[49] Recently, the same group designed and fabricated visible light photocatalysts by grafting Cu(II) on the surfaces of $TiO_2$ and $WO_3$ particles.[50]

It is hypothesized that the solid−solid interface is a key structural feature that facilitates charge separation and enhances photocatalytic efficiency, and may be the locus of photocatalytic "hot spots".[6] Previously, we have demonstrated that highly photoactive, tetrahedrally coordinated Ti sites can be prepared in the interfacial region between anatase and rutile in mixed-phase $TiO_2$ nanocomposites.[14] As highly active centers, the interfacial Ti sites in mixed-phase $TiO_2$ provided additional adsorption sites which induced the formation of charge-transfer complexes.[51,52] In this present study, we show that interfacial Ti−O−Cu linkages exist in a $CuO-TiO_2$ nanocomposite with

a very low copper loading which demonstrated enhanced photocatalytic activity. Substitutional $Cu^{2+}$ sites, which exist as interfacial Ti−O−Cu linkages and are characterized by the resonances at $g_{\|} = 2.33$ and $g_{\perp} = 2.07$ in the EPR spectrum shown in Figure 5, may be the active sites responsible for the improved photoactivity of 0.1% $CuO-TiO_2$ relative to pure $TiO_2$ nanoparticles. One possible mechanism for the improved photocatalytic activity, in our opinion, is that the surface/interfacial $Cu^{2+}$ sites in the 0.1% $CuO-TiO_2$ nanocomposite function as unique adsorption sites for MB and facilitate the subsequent photocatalytic degradation. The degree of electronic interactions between semiconductor surface and the reactant molecules is considered as a critical factor in a "Direct−Indirect" model to explain the kinetics of photocatalytic processes.[53]

## 4. Conclusions

A series of photoactive $CuO-TiO_2$ nanocomposites were prepared via a deposition precipitation method as coupled semiconductors bearing strong electronic interaction between the two phases. Since the band edges of $TiO_2$ bracket those of CuO, coupling between CuO and $TiO_2$ led to decreased photocatalytic efficiency due to the charge transfer from $TiO_2$ to CuO and subsequent charge recombination. Surprisingly, a $CuO-TiO_2$ nanocomposite with a very low copper loading (0.1 wt %) demonstrated improved photoactivity relative to pure $TiO_2$. Studies by EPR spectroscopy revealed the presence of highly dispersed CuO clusters and substitutional $Cu^{2+}$ sites in the 0.1% $CuO-TiO_2$. The existence of such sites is believed to account for the enhanced photoactivity of this nanocomposite. The experimental results highlight the importance of interfacial morphology in the photocatalytic properties of $TiO_2$-based nanocomposites. In addition, this study illustrates a new approach to improve the photoactivity of $TiO_2$ by controlled surface modification using a narrower-band semiconductor, which in bulk form serves as a recombination center.

**Acknowledgment.** The authors thank the U.S. Department of Energy (DE-FG02-03ER15457/A003 and DE-AC02-06CH11357) for funding the research described in this paper, and Professor Joseph T. Hupp and Karen Mulfort of Chemistry Department at Northwestern University for their help on surface area measurements. Materials characterization was performed in MRSEC, NUANCE, and ASL at Northwestern University.

## References and Notes

(1) Chen, X.; Mao, S. S. *Chem. Rev.* **2007**, *107*, 2891.
(2) Thompson, T. L.; Yates, J. T., Jr. *Chem. Rev.* **2006**, *106*, 4428.
(3) Carp, O.; Huisman, C. L.; Reller, A. *Prog. Solid State Chem.* **2004**, *32*, 33.
(4) Anpo, M.; Takeuchi, M. *J. Catal.* **2003**, *216*, 505.
(5) Diebold, U. *Surf. Sci. Rep.* **2003**, *48*, 53.
(6) Li, G.; Gray, K. A. *Chem. Phys.* **2007**, *339*, 173.
(7) Rajeshwar, K.; de Tacconi, N. R.; Chenthamarakshan, C. R. *Chem. Mater.* **2001**, *13*, 2765.
(8) Kamat, P. V. *Pure Appl. Chem.* **2002**, *74*, 1693.
(9) Pichat, P.; Borgarello, E.; Disdier, J.; Herrmann, J. M.; Pelizzetti, E.; Serpone, N. *J. Chem. Soc., Faraday Trans. 1* **1988**, *84*, 261.
(10) Serpone, N.; Maruthamuthu, P.; Pichat, P.; Pelizzetti, E.; Hidaka, H. *J. Photochem. Photobiol. A* **1995**, *85*, 247.
(11) Shimodaira, Y.; Kudo, A.; Kobayashi, H. *Chem. Lett.* **2007**, *36*, 170.
(12) Hurum, D. C.; Agrios, A. G.; Gray, K. A.; Rajh, T.; Thurnauer, M. C. *J. Phys. Chem. B* **2003**, *107*, 4545.
(13) Hurum, D. C.; Agrios, A. G.; Crist, S. E.; Gray, K. A.; Rajh, T.; Thurnauer, M. C. *J. Electron Spectrosc. Relat. Phenom.* **2006**, *150*, 155.
(14) Li, G.; Dimitrijevic, N.; Chen, L.; Nichols, J.; Rajh, T.; Gray, K. A. *J. Am. Chem. Soc.* **2008**, *130*, 5402.
(15) Xu, Y.; Schoonen, M. A. A. *Am. Mineral.* **2000**, *85*, 543.
(16) Slamet; Nasution, H. W.; Purnama, E.; Kosela, S.; Gunlazuardi, J. *Catal. Commun.* **2005**, *6*, 313.
(17) Tseng, I. H.; Chang, W. C.; Wu, J. C. S. *Appl. Catal. B* **2002**, *37*, 37.
(18) Tseng, I. H.; Wu, J. C. S. *Catal. Today* **2004**, *97*, 113.
(19) Saponjic, Z. V.; Dimitrijevic, N. M.; Poluektov, O. G.; Chen, L.; Wasinger, E.; Welp, U.; Tiede, D. M.; Zuo, X.; Rajh, T. *J. Phys. Chem. B* **2006**, *110*, 25441.
(20) Li, G.; Gray, K. A. *Chem. Mater.* **2007**, *19*, 1143.
(21) You, X.; Chen, F.; Zhang, J.; Anpo, M. *Catal. Lett.* **2005**, *102*, 247.
(22) Li, G.; Chen, L.; Dimitrijevic, N.; Gray, K. A. *Chem. Phys. Lett.* **2008**, *451*, 75.
(23) Kudo, A.; Niishiro, R.; Iwase, A.; Kato, H. *Chem. Phys.* **2007**, *339*, 104.
(24) Zhang, W.; Li, Y.; Zhu, S.; Wang, F. *Catal. Today* **2004**, *93−95*, 589.
(25) Xu, B.; Dong, L.; Chen, Y. *J. Chem. Soc., Faraday Trans.* **1998**, *94*, 1905.
(26) Chary, K. V. R.; Sagar, G. V.; Srikanth, C. S.; Rao, V. V. *J. Phys. Chem. B* **2007**, *111*, 543.
(27) Chary, K. V. R.; Sagar, G. V.; Naresh, D.; Seela, K. K.; Sridhar, B. *J. Phys. Chem. B* **2005**, *109*, 9437.
(28) Reddy, B. M.; Sreekanth, P. M.; Yamada, Y.; Xu, Q.; Kobayashi, T. *Appl. Catal. A* **2002**, *228*, 269.
(29) Sykes, E. C. H.; Tikhov, M. S.; Lambert, R. M. *J. Phys. Chem. B* **2002**, *106*, 7290.
(30) Abad, J.; Rogero, C.; Mendez, J.; Lopez, M. F.; Martin-Gago, J. A.; Roman, E. *Surf. Sci.* **2006**, *600*, 2696.
(31) Xia, J.; Masaki, N.; Jiang, K.; Yanagida, S. *J. Phys. Chem. B* **2006**, *110*, 25222.
(32) Ardelean, I.; Peteanu, M.; Ciceo-Lucacel, R.; Bratu, I. *J. Mater. Sci.: Mater. Electron.* **2000**, *11*, 11.
(33) Sreenivasu, D.; Chandramouli, V. *Bull. Mater. Sci.* **2000**, *23*, 281.
(34) Ciorcas, F.; Mendiratta, S. K.; Ardelean, I.; Valente, M. A. *Eur. Phys. J.* **2001**, *20*, 235.
(35) Martinez-Arias, A.; Fernandez-Garcia, M.; Soria, J.; Conesa, J. C. *J. Catal.* **1999**, *182*, 367.
(36) Gerritsen, H. J.; Sabisky, E. S. *Phys. Rev.* **1962**, *125*, 1853.
(37) Amorelli, A.; Evans, J. C.; Rowlands, C. C. *J. Chem. Soc., Faraday Trans. 1* **1989**, *85*, 4111.
(38) Darab, J. G.; MacCrone, R. K. *Phys. Chem. Glasses* **1991**, *32*, 91.
(39) Harrison, P. G.; Bailey, C.; Daniell, W.; Zhao, D. D.; Ball, I. K.; Goldfarb, D.; Lloyd, N. C.; Azelee, W. *Chem. Mater.* **1999**, *11*, 3643.
(40) Hurum, D. C.; Gray, K. A.; Rajh, T.; Thurnauer, M. C. *J. Phys. Chem. B* **2004**, *108*, 16483.
(41) Hurum, D. C.; Gray, K. A.; Rajh, T.; Thurnauer, M. C. *J. Phys. Chem. B* **2005**, *109*, 977.
(42) Anpo, M.; Thomas John, M. *Chem. Commun.* **2006**, 3273.
(43) Arai, Y.; Tanaka, K.; Khlaifat, A. L. *J. Mol. Catal. A* **2006**, *243*, 85.
(44) Notari, B.; Willey, R. J.; Panizza, M.; Busca, G. *Catal. Today* **2006**, *116*, 99.
(45) Gartner, M.; Dremov, V.; Muller, P.; Kisch, H. *ChemPhysChem* **2005**, *6*, 714.
(46) Puzenat, E.; Pichat, P. *J. Photochem. Photobiol. A* **2003**, *160*, 127–133.
(47) Lin, W.; Frei, H. *J. Am. Chem. Soc.* **2005**, *127*, 1610.
(48) Lin, W.; Frei, H. *J. Phys. Chem. B* **2005**, *109*, 4929.
(49) Nakamura, R.; Okamoto, A.; Osawa, H.; Irie, H.; Hashimoto, K. *J. Am. Chem. Soc.* **2007**, *129*, 9596.
(50) Irie, H.; Miura, S.; Kamiya, K.; Hashimoto, K. *Chem. Phys. Lett.* **2008**, *457*, 202.
(51) Agrios, A. G.; Gray, K. A.; Weitz, E. *Langmuir* **2003**, *19*, 1402.
(52) Agrios, A. G.; Gray, K. A.; Weitz, E. *Langmuir* **2004**, *20*, 5911.
(53) Monllor-Satoca, D.; Gomez, R.; Gonzalez-Hidalgo, M.; Salvador, P. *Catal. Today* **2007**, *129*, 247.

JP8068392